Construction and Building Materials 284 (2021) 122834

Contents lists available at ScienceDirect

Construction and Building Materials

journal homepage: www.elsevier.com/locate/conbuildmat

Effect of curing relative humidity on mechanical properties of engineered cementitious composites at multiple scales

Mingfeng Xu [a], Jing Yu [b], Jian Zhou [a], Yi Bao [c], Victor C. Li [d,*]

[a] School of Civil and Transportation Engineering, Hebei University of Technology, Tianjin 300401, China
[b] School of Civil Engineering, Sun Yat-Sen University, Guangzhou 510275, China
[c] Department of Civil, Environmental and Ocean Engineering, Stevens Institute of Technology, Hoboken, NJ 07030, USA
[d] Department of Civil and Environmental Engineering, University of Michigan, Ann Arbor, MI 48109-2125, USA

HIGHLIGHTS

- Impacts of relative humidity (RH) on tensile properties of ECC is elucidated.
- Its mechanism is revealed by the response of matrix and fiber/matrix interface to RH.
- It advances the standardization of ECC preparation of property characterization.

ARTICLE INFO

Article history:
Received 13 June 2020
Received in revised form 15 February 2021
Accepted 23 February 2021

Keywords:
Engineered Cementitious Composites (ECC)
Relative humidity (RH)
Mechanical properties
Multi-scale
Micromechanical modeling

ABSTRACT

In recent years, broad interests in ductile Engineered Cementitious Composites (ECC) have been accompanied by increasing amount of laboratory investigations of this material. Both wet and air curing have been applied in the preparation of specimens. However, the effect of curing condition on mechanical properties of ECC has yet to be elucidated. This research attempts to fill this knowledge gap. Specifically, experiments were conducted to investigate property changes at different length scales under three curing relative humidity (RH) levels. Macroscopic properties including composite first crack strength, ultimate tensile strength and strain capacity, and crack pattern of ECC reinforced with PVA fibers were recorded. As well, matrix fracture toughness and fiber/matrix interface properties were measured. Correlation of macro-properties and micromechanical parameters was interpreted using a previously developed micromechanical model. The changes of tensile properties and crack pattern were found traceable to RH effects on the matrix and fiber/matrix interface properties. The findings of this study reveal the underlying mechanisms of property differences in specimens cured under different RH. The knowledge gained provides a better understanding of the effects of curing conditions on ECC specimens used in property characterization, and is particularly relevant to maintaining consistency in standardized testing of ECC.

1. Introduction

Engineered Cementitious Composites (ECC) belong to the family of fiber-reinforced cementitious composites with high tensile ductility (3–7%) and intrinsically tight crack widths (typically less than 100 μm) with moderate fiber content (below 2 vol%) [1]. Originally developed for earthquake resistant structures, ECC is currently emerging in building, transportation, water and energy infrastructures for enhanced resiliency, durability and sustainability [2–5]. Considering the high hydration heat and high environmental impact of ordinary Portland cement, green ECC incorporating high volumes of fly ash (up to 85 wt% of the binder) has also been designed to maximize the material greenness and infrastructure sustainability [6–9].

To attain high tensile ductility and tight crack width, ECC is designed based on synergistic interactions between fiber, matrix, and fiber/matrix interface. Both matrix and fiber/matrix interface properties are known to be affected by the hydration of the cementitious binder. As hydration continues, the matrix fracture toughness increases, leading to a higher first crack strength but reducing the composite ductility [10]. Hydration of binder also contributes to the maturity of the fiber/matrix interface, increasing the bonding properties. Fiber/matrix interfacial bond is responsible

* Corresponding author.
E-mail address: vcli@umich.edu (V.C. Li).

https://doi.org/10.1016/j.conbuildmat.2021.122834
0950-0618/

for desirable composite behavior, but excessive interfacial bond could lead to a loss of tensile strain capacity [11].

A large number of studies have already been reported on the mechanical and durability performance of normal concrete cured under various relative humidity (RH) levels. It has been found that the increase in RH and moisture curing period results in higher compressive and tensile strength, as well as lower sorptivity and permeability in concrete [12–15]. For concrete with supplementary cementing materials, the impact of RH is even more significant, as a longer moisture curing period with higher RH results in more strength contribution from the pozzolanic reaction [12]. The rate of hydration of cementitious binder highly depends on the relative humidity (RH), and can affect the pore structure and hydration products, which directly impact concrete mechanical and durability properties [16].

In some studies of ECC, specimens were prepared using air curing [17–19], while other studies involve specimens prepared under water curing [6,20,21]. Despite the well-known fact that RH affects the performance of cementitious materials in general, the literature on the impact of RH curing conditions on the mechanical properties of ECC is lacking. It is hypothesized that RH curing conditions have a direct impact on the mechanical properties and especially the tensile properties of ECC specimens. Specifically, RH curing condition is expected to influence the facture toughness of the matrix material and the bond properties of the fiber/matrix interface. Depending on their delicate balance, modification of matrix and fiber/matrix interface properties may improve or diminish the composite tensile properties, especially the tensile strength and ductility. A systematic study of the influence of RH curing conditions on the macro and micro properties of ECC would allow a deeper understanding of how relative humidity works on these length scales, and their linkages.

This study investigates the effect of different curing RH on the mechanical properties of ECC specimens containing high-volume fly ash and reinforced with PVA fibers. Three curing RH conditions were adopted. Immediately after a curing period of 7 days, 28 days and 60 days, ECC specimens were examined for their compressive and tensile properties, especially the tensile stress–strain responses. Residual crack pattern was also studied for the set of specimens cured for 28 days. Additionally, the matrix fracture toughness and the fiber /matrix interface bond properties were measured for specimens cured in the same three RH environments for 28 days. The differences in macroscopic properties of ECC cured under different RH conditions were interpreted in terms of the changes in matrix toughness and fiber/matrix interface properties under different RH conditions. The objective of this study is to discern the impact of RH on ECC tensile properties, and to gain a deeper understanding of the micro-mechanisms underlying the macroscopic observations in tensile behavior.

2. Experimental program

2.1. Raw materials and mix proportions

To investigate the mechanical properties of ECC as affected by RH during curing, two mix proportions (fly ash/cement ratio (FA/C) ranged from 1.2 to 2.2) developed in previous studies [17,22] were adopted (Table 1). In these mixes, the water/binder ratio (W/(C + FA)) and sand/binder (S/(C + FA)) were fixed at 0.25 and 0.36, respectively. Type I Portland cement (C) and ASTM Class F fly ash (FA) were used as the binder. The chemical and physical properties of cement and fly ash are listed in Table 2. The cement had a specific surface area of 376 m^2/kg. The fly ash had a water requirement of control of 94%. The strength activity index of the fly ash was 91% at 7 days and 97% at 28 days. Fine siliceous sand with an average grain size of 75 μm were adopted as fine aggregates. The physical properties of the PVA fiber (Kuraray K-II) were listed in Table 3. The volume fraction of PVA fiber was fixed at 2%. To ensure consistent flowability of the mixtures, a commercial polycarboxylate-based superplasticizer (SP) was used to achieve a slump flow diameter of 165 ± 5 mm according to ASTM C1437 [23].

2.2. Specimen preparation and curing conditions

A Hobart HL800 mortar mixer was used to prepare ECC. The fresh mixture was cast into molds, and covered with plastic sheets for 24 h to prevent moisture loss. After demolding, the test specimens were cured in the RH conditions of 25 ± 5% (RH25), 55 ± 5% (RH55) and 95 ± 5% (RH95), until the tests at 7, 28, and 60 days, respectively. The curing conditions are shown in Fig. 1. The relative humidity in lab environment stayed within 25 ± 5% during the curing period, controlled by the lab air conditioning system. Sealed chambers with hygrometers inside were used to manually control the curing humidity. To obtain a curing humidity of 55 ± 5%, desiccants (silica gels) were used to absorb the extra moisture released by specimens. To obtain a curing humidity of 95 ± 5%, wet paper towels were used to release moisture into the sealed chamber. The frequency of changing desiccant or wet paper towels in the sealed box depends on the relative humidity shown on the hygrometers. The curing temperature was automatically controlled at 20 ± 1℃, by the lab air conditioning system.

2.3. Experimental procedures

2.3.1. Compressive test

To determine the compressive strength, cube specimens (50 mm × 50 mm × 50 mm) recommended by ASTM 109C [24] were tested using a loading machine (FORNEY F50) with a 10 N resolution at a loading rate of 0.14 MPa/s.

2.3.2. Uniaxial tensile test and crack pattern characterization

The tensile behavior was determined by uniaxial tensile test using dogbone shaped specimens, as recommended by JSCE [25]. The test setup is shown in Fig. 2(a). Tensile test was conducted under displacement control and the displacement rate was kept constant at 0.5 mm/min [25]. To measure the extension of specimen under uniaxial tension, two external linear variable displacement transducers (LVDT) were attached to both sides of the dogbone specimens. The gage length was 80 mm. Tensile load was monitored using a load cell. The slope of initial linear stage of the tensile stress-strain curve of the composites was used to estimate the composite Young' modulus E_c. The first crack stress σ_{fc} of ECC was determined from the stress-strain relation where it first deviates from linearity.

Table 1
Mix proportions.

Material	C	FA	Sand	SP	W/(C + FA)	S/(C + FA)	Fiber (vol.%)
FA1.2-ECC	1	1.2	0.80	0.004	0.25	0.36	2
FA2.2-ECC	1	2.2	1.16	0.006	0.25	0.36	2

Table 2
Chemical composition and physical properties of cement and fly ash.

	C	FA
SiO_2 (%)	19.6	39.77
Al_2O_3(%)	4.8	20.00
Fe_2O_3(%)	2.9	9.74
CaO (%)	63.5	18.88
MgO (%)	2.2	3.67
SO_3(%)	2.6	1.95
Na_2O equivalent (%)*	0.57	2.02
Loss of ignition (%)	2.6	0.86
Density (g/cm^3)	3.15	2.71

* Na_2O equivalent = Na_2O + 0.658K_2O.

The multiple crack pattern after tensile test was analyzed using the dogbone specimens cured for 28 days. The residual crack number and width measured on the surface of the specimen after tensile tests were recorded, following the method reported in [7,26–29]. Three straight lines were drawn on each specimen as reference lines with cracks crossing these lines more or less perpendicularly (Fig. 3(a)). Microcracks were measured parallel to the tensile load direction along the reference lines (Fig. 3(b)). "Residual crack" here indicates that the crack width and number were measured/-counted when the uniaxial tensile load was taken off, after the specimens have been tested to failure. The width of the failure crack that led to tension-softening of the tensile specimen was not included in this data.

2.3.3. Single fiber tensile test

To investigate the mechanisms behind the influence of curing RH on tensile properties of ECC, a series of tests were conducted on the matrix (ECC without fibers) and fiber/matrix interface using specimens cured under the same three RH conditions (as for the composite specimens) for 28 days. Single fiber pullout test was conducted to measure the interfacial chemical bond G_d and frictional bond τ_0 following the recommended procedure in Redon *et al.* [30]. The embedment length of the fiber was controlled around 0.8 ~ 1.0 mm to ensure a full debonding. Before the pullout test, the bottom surface of the thin specimen was first glued on the mount of the setup. The exposed fiber end was then glued onto the aluminum plate that was tensioned by the upper grips (Fig. 2(b)). A 10-N load cell was used to capture the pullout force. The pullout test was conducted under a displacement control of 0.5 mm/min. The displacement of the pullout curves is given by the displacement of the actuator.

A typical pulled-out load–displacement curve is shown in Fig. 4. It can be divided into three stages. Initially, a stable fiber debonding process occurs at the fiber/matrix interface, until the load increases to P_a. Then, the load suddenly drops from P_a to P_b, indicating a complete chemical debond along the full length of the embedded fiber in the matrix. Finally, only the frictional force provides the fiber resisting load. As the PVA fiber undergoes sliding accompanied by surface abrasion, the fibrils formed may jammed the exiting of the fiber from the matrix, resulting in a slip-hardening phenomenon. This competes with the effect of continuous reduction of the remaining embedment length as the fiber pulls out. Depending on the initial embedment length, the fiber may break before complete pull-out [30]. Based on the P_a and P_b values on the load–displacement curve, the chemical bond G_d and frictional bond τ_0 are calculated using Eqn (1) and Eqn (2).

$$G_d = \frac{2(P_a - P_b)^2}{\pi^2 E_f d_f^3} \tag{1}$$

$$\tau_0 = \frac{P_b}{\pi d_f L_e} \tag{2}$$

where E_f is the fiber axial Young's modulus; d_f is the fiber diameter; L_e is the initial fiber embedded length. Considering the typical large scatter of the pull-out test, 30 specimens were adopted for each test condition, and the results were averaged.

2.3.4. Three point bending test

Matrix fracture toughness K_m was also measured using three-point bending test recommended by ASTM E399 [31]. Its test setup was shown in Fig. 2(c). The size of the beam specimen for K_m testing was 304.8 mm × 76.2 mm × 38.1 mm, with a loading span of 254.0 mm between supports. The notch depth to height ratio was 0.4.

3. Results and discussion

3.1. Compressive strength

The compressive strengths of both FA2.2-ECC and FA1.2-ECC increase with increasing curing RH, and this trend is consistent for the results from all curing times (Fig. 5). During the curing process, moisture present in the capillary pores vaporizes continuously until an equilibrium with the ambient conditions is attained. This process may take as much as three years for the inner humidity to drop down to 50% [14]. A lower curing RH can accelerate the moisture releasing rate because of a higher initial moisture concentration gradient. A higher resulting moisture gradient will therefore reduce the degree of hydration and pozzolanic reaction, and also lead to a reduction in the volume of small capillary pores and a corresponding increase in the volume of larger pores [12,15]. This negative effect of low humidity on hydration product and microstructure is expected to apply to ECC, and is well reflected in the compressive strength data shown in Fig. 5. The compressive strength is significantly lower under the curing condition of lower RH.

As expected, increasing fly ash content reduces the compressive strength of ECC mixtures, even for longer curing time. The reason behind this has been well studied [12,32]. The lower reactivity of low-calcium Class F fly ashes relative to that of cement clinker phase is responsible for the lower compressive strength.

3.2. Uniaxial tensile properties

Both ECC mixes show tensile strain-hardening behavior under all curing conditions used in this study. Increase in RH enhances the first cracking strength and ultimate tensile strength of ECC, but depresses the tensile ductility (Fig. 6). These properties are summarized in Table 4. For both mixes, the tensile strain capacity decreases as the curing time increases from 7 to 60 days.

Table 3
Nominal properties of PVA fibers.

Length (mm)	Diameter (μm)	Elongation(%)	Density (kg/m^3)	Young's Modulus (GPa)	Normal Strength (MPa)
12	39	6	1300	42.8	1600

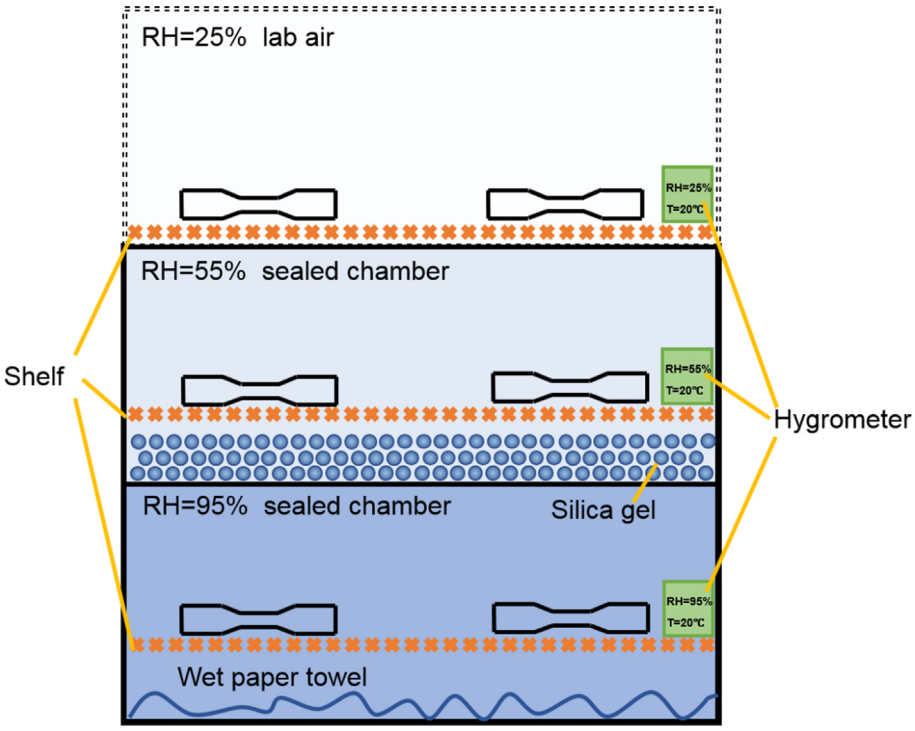

Fig. 1. Schematic drawing of the curing chamber with relative humidity of 25%, 55% and 95%.

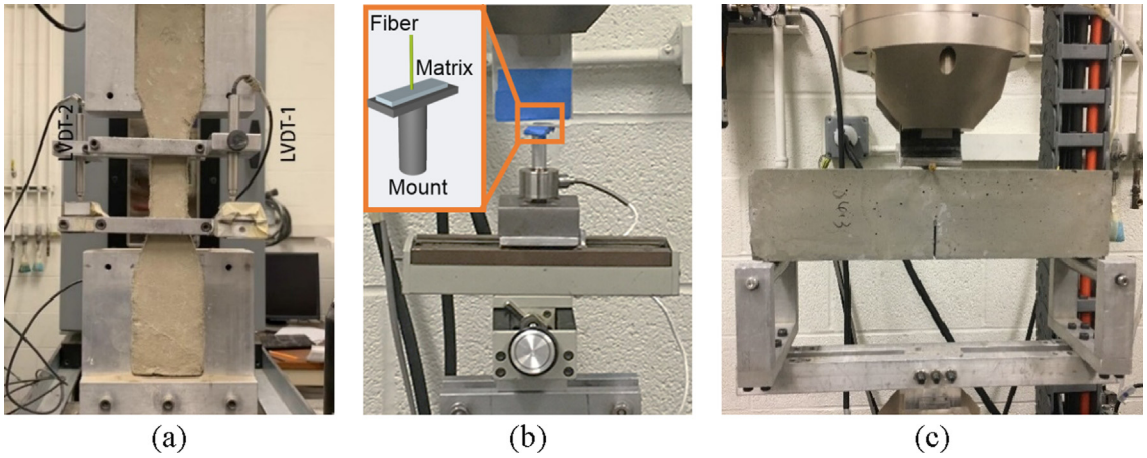

Fig. 2. Test setup: (a) Uniaxial tensile test; (b) Single-fiber tensile test; (c) Three-point bending test.

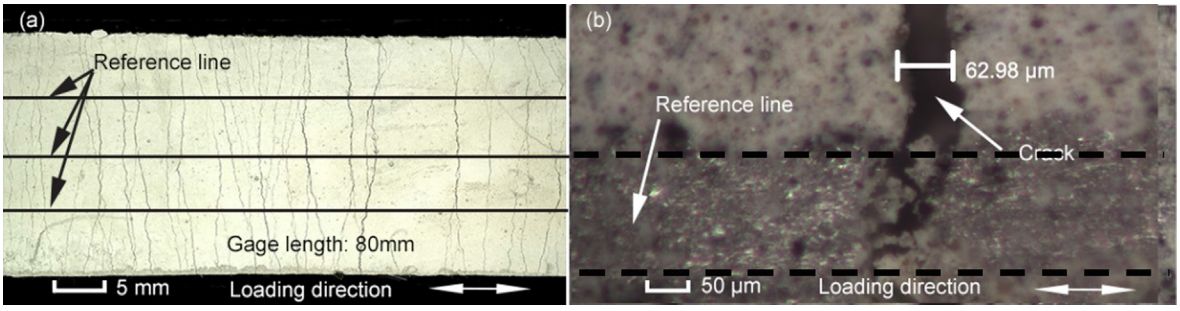

Fig. 3. Residual crack measurement: (a) Recording of surface crack pattern over the gage length of a dogbone specimen; (b) Measurement of the width of microcracks crossing the reference lines.

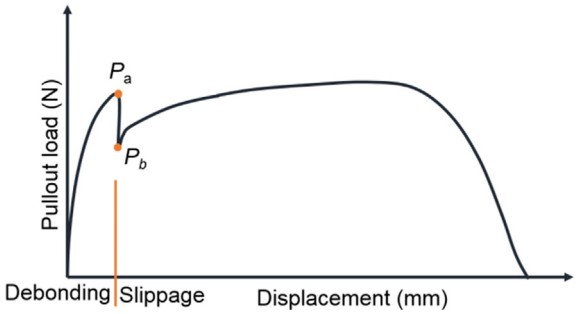

Fig. 4. General profile of a curve for a single fiber pulled-out test.

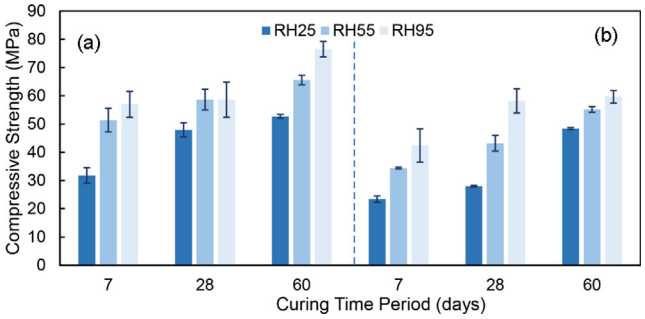

Fig. 5. Compressive strength of (a) FA1.2-ECC and (b) FA2.2-ECC under various RH conditions at different times. In this study, the test age is the same as the curing time.

3.3. Residual crack pattern

The average residual crack width is found to increase while the number of cracks within the specimen gage length is found to decrease with the increase in RH (Table 5).

The crack number and crack width are two basic factors contributing to the tensile strain capacity. Fig. 7 shows the residual sequential cracks of ECC cured under RH of 25 ± 5%, 55 ± 5% and 95 ± 5% for 28 days. As shown in Table 5, the significant decrease in crack number overwhelms the effect of the slight increase in crack width, leading to an overall decrease in tensile strain capacity as the curing RH increases.

It should be noted that the crack widths were measured after the specimens have been loaded to failure. For the specimens exposed to higher RH, the peak loads were also higher (Fig. 6), implying that the bridged cracks experienced a higher load. A better way for crack width comparison might be to evaluate the crack pattern under the same tensile load level. Even though the residual crack width increases with high humidity, the largest crack width is 24.04 μm and all remain less than 50 μm, which is still favorable for the self-healing behavior of ECC [33].

The residual crack width and crack number (with a crack width interval of 10 μm) of the dogbone specimens is plotted in the histogram in Fig. 8 to show the crack width distributions, based on microscopy observations. In previous studies, probability density function (PDF) of the lognormal distribution was adopted to best fit the observed crack width distributions [17,22]. Detailed information about the fitting process can be found in reference [17,22]. The plotted best-fit curve using lognormal PDF is obtained

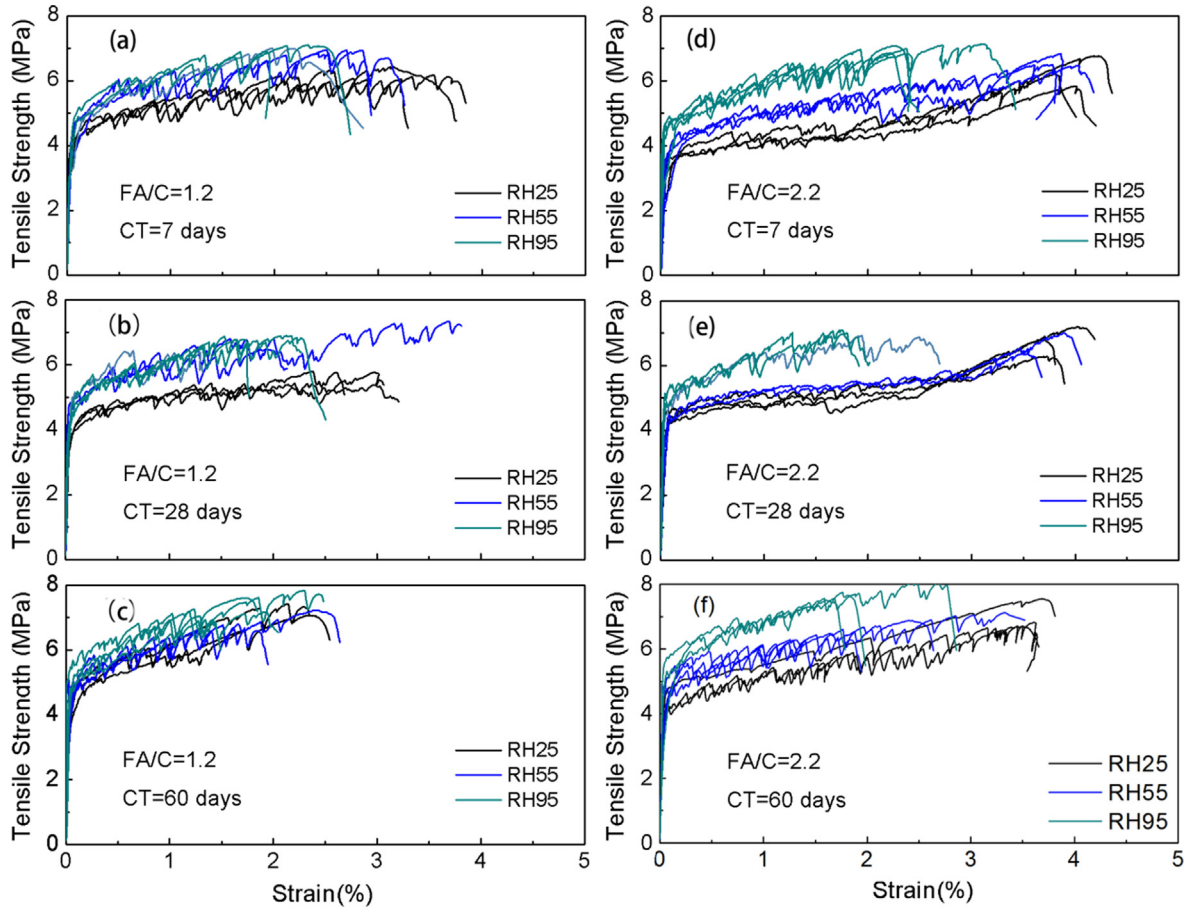

Fig. 6. All ECCs tested show tensile strain hardening. First crack and ultimate tensile strength increase but tensile strain capacity decreases with increasing curing RH and curing time (CT).

Table 4
Tensile test results of ECC cured under different curing RH conditions.

Curing Conditions		FA/C = 1.2			FA/C = 2.2		
		First cracking strength (MPa)	Ultimate tensile strength (MPa)	Tensile strain capacity (%)	First cracking strength (MPa)	Ultimate tensile strength (MPa)	Tensile strain capacity (%)
7d	RH25	4.00 ± 0.08	6.22 ± 0.16	3.35 ± 0.24	2.98 ± 0.28	6.27 ± 0.38	4.00 ± 0.15
	RH55	4.16 ± 0.18	6.97 ± 0.03	2.51 ± 0.27	3.74 ± 0.11	6.60 ± 0.16	3.87 ± 0.12
	RH95	4.40 ± 0.56	6.98 ± 0.08	2.12 ± 0.21	4.24 ± 0.17	7.00 ± 0.10	2.43 ± 0.38
28d	RH25	4.07 ± 0.04	5.65 ± 0.19	3.12 ± 0.65	3.96 ± 0.44	6.76 ± 0.37	3.80 ± 0.16
	RH55	4.16 ± 0.06	6.77 ± 0.36	2.29 ± 0.88	4.05 ± 0.02	6.72 ± 0.36	3.69 ± 0.20
	RH95	4.40 ± 0.17	6.89 ± 0.02	1.63 ± 0.30	4.71 ± 0.30	7.01 ± 0.07	1.83 ± 0.08
60d	RH25	4.35 ± 0.36	6.82 ± 0.24	2.46 ± 0.75	4.40 ± 0.26	7.00 ± 0.44	3.63 ± 0.09
	RH55	4.73 ± 0.06	6.87 ± 0.26	2.16 ± 0.79	4.71 ± 0.24	7.10 ± 0.43	3.23 ± 0.87
	RH95	4.96 ± 0.09	7.41 ± 0.32	1.63 ± 0.37	5.13 ± 0.55	7.78 ± 0.23	1.94 ± 0.36

Table 5
Averaged residual crack width and number of cracks in the two ECC mixtures cured under various RH conditions at age of 28 days.

	FA/C = 1.2			FA/C = 2.2		
	RH25	RH55	RH95	RH25	RH55	RH95
Width (μm)	14.2	22.15	24.04	10.68	12.62	16.11
Number	46	27	18	69	55	39

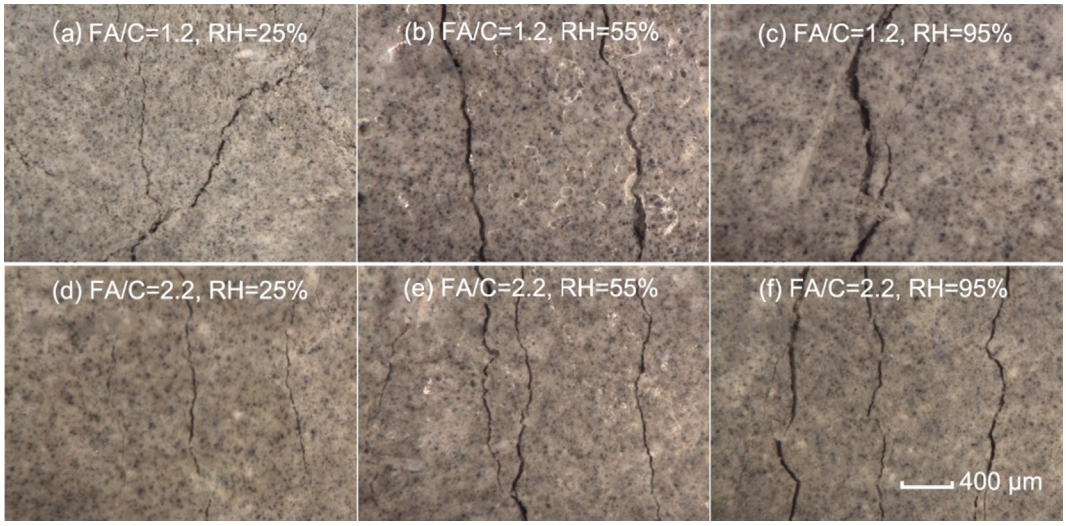

Fig. 7. Optical photos of residual crack pattern of ECC cured under various RH for 28 days. Increase in crack width can be observed in these photos for specimens cured at higher RH.

by scaling up the probability density function by the total residual cracks number and the interval of the histogram (10 μm) in Fig. 8. The best fitting curve is meaningful only at the crack widths which are multiples of 10 μm. The observed crack width distribution is consistent with those reported by van Zijl *et al.*[34].

In Fig. 9, continuous fitting curves are used to characterize the crack patterns of specimens subjected to various curing conditions. Specimens cured under higher RH tend to have crack patterns of loosely spaced cracks with wider crack width. This observation applies to both mixes but is particularly evident for the mix with lower FA content.

3.4. Underlying mechanisms of observed dependence of ECC tensile properties on curing RH

In order to gain a deeper insight into the mechanisms that govern the macroscopic tensile behavior of ECC as related to curing RH, a previously developed micromechanical model is used in combination with micromechanical parameters derived from the current study. In the following, the relevant basics of the micromechanical model is briefly highlighted. Experimentally determined interfacial parameters τ_0 and G_d, and matrix parameter K_m as a function of curing RH are presented. The modeled fiber bridging relation $\sigma(\delta)$ is then used to interpret the observed dependence of tensile strain capacity and crack pattern on curing RH.

3.4.1. Basics of micromechanical model

According to the design theory of ECC, the strength criterion (Eqn (3)) and the energy criterion (Eqn (4)) should be satisfied to ensure robust strain hardening [11,35]. The strength criterion requires that the first cracking strength σ_{fc} must not exceed the maximum fiber bridging strength σ_0, which assures that cracks initiated during composite strain-hardening will not result in catastrophic loss of load carrying capacity on the crack plane. After a crack is initiated from a pre-existing flaw, the propagating crack must remain flat with limited opening to maintain the integrity of the bridging fibers. Otherwise, fibers will rupture or pull out as crack width widens during propagation. To ensure the flat crack

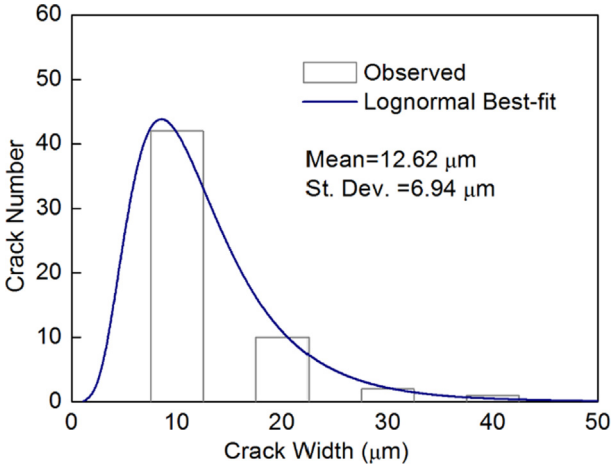

Fig. 8. Observed and best-fitting lognormal distributions for crack width distribution of ECC (FA/C = 2.2, RH = 25 ± 5%, 28d). The observed residual crack pattern fits well with lognormal curve.

propagation mode, the energy criterion requires a crack tip toughness J_{tip} lower than the complementary energy J'_b.

$$\sigma_{fc} \leqslant \sigma_0 \tag{3}$$

$$J_{tip} \leqslant \sigma_0\delta_0 - \int_0^{\delta_0} \sigma(\delta)d\delta = J'_b \tag{4}$$

where $J_{tip} = K_m^2/E_m$ is the crack opening corresponding to the maximum bridging stress σ_0, K_m is the matrix fracture toughness, and E_m is the Young's Modulus of the matrix, assumed to be approximately equal to the measured K_c due to the low fiber content of 2%. The crack-bridging $\sigma(\delta)$ constitutive law is governed [36] by a set of micromechanics parameters, including interfacial chemical bond G_d, interfacial frictional bond τ_0, slip-hardening coefficient β, as well as matrix modulus E_m, fiber content V_f, and fiber diameter d_f. To satisfy the two strain-hardening criteria, and consequently to obtain robust tensile ductility in ECC, a delicate balance of fiber, matrix, and fiber/matrix interfaces is necessary [11].

3.4.2. Influence of RH on micromechanical parameters τ_0, G_d and K_m

The fiber/matrix interface parameters determined from single fiber pull out tests are summarized in Fig. 10 and Fig. 11. The specimens were cured for 28 days and tested immediately after curing. Despite the large data variations, typical of the single fiber pull-out test [6,11,26,37], a general ascending trend of frictional bond with increase in curing RH is observed, particularly for the FA/C = 1.2 mix. It is known that frictional bond τ_0 is closely related to the

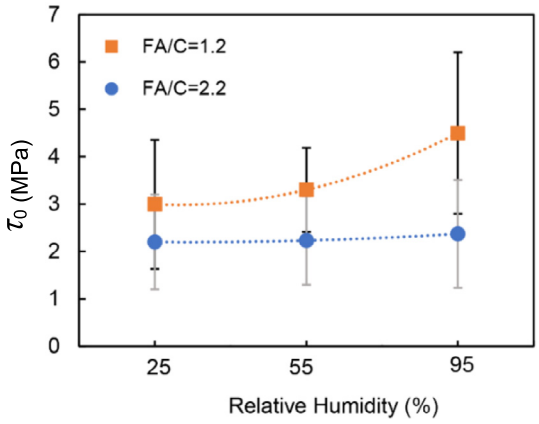

Fig. 10. Influence of curing RH on the fiber/matrix interfacial frictional bond τ_0.

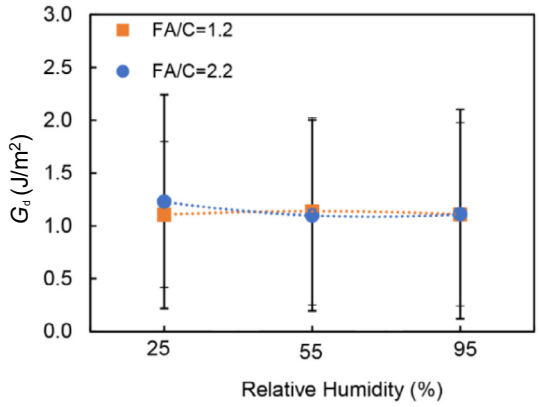

Fig. 11. Influence of curing RH on the fiber/matrix interfacial chemical bond G_d.

packing density and stiffness of the interfacial transition zone [6]. Thus, high τ_0 at high RH indicates a denser microstructure of the interfacial transition zone, as well as strong resistance against fiber pull-out. Contrary to the increasing trend of frictional bond with curing RH, the chemical bond G_d exhibits little dependence on curing RH (Fig. 11). The matrix fracture toughness K_m does show a strong dependence on RH curing, as shown in Fig. 12.

3.4.3. Interpretation of observed curing RH dependence of strain capacity and crack pattern

Based on the measured fiber/matrix interfacial properties, the $\sigma(\delta)$ curves of ECC under various curing RH were computed following Yang [36] and shown in Fig. 13. The calculated complementary

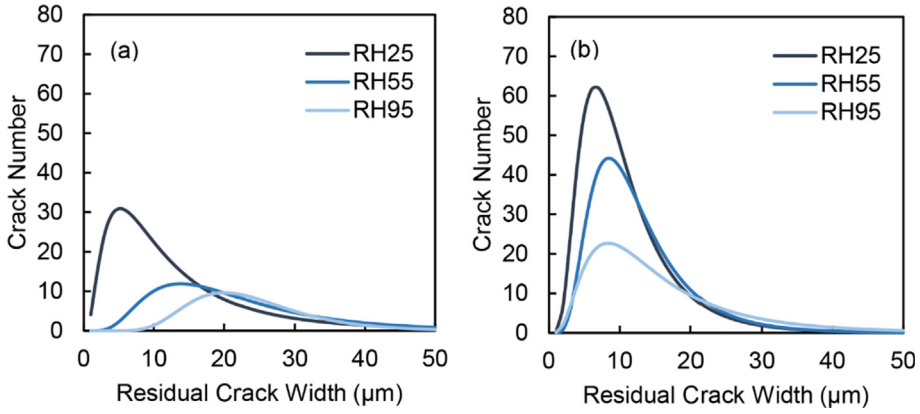

Fig. 9. Crack pattern of ECCs under various RH conditions: (a) FA/C = 1.2; (b) FA/C = 2.2. Crack number decreases while crack width increases with RH for both ECC mixes.

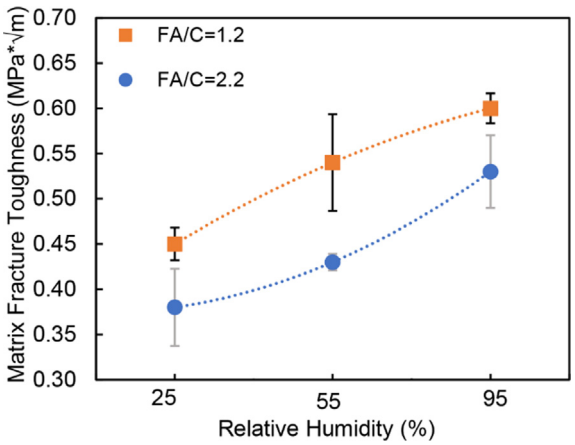

Fig. 12. Influence of curing RH on the matrix fracture toughness K_m.

energy of fiber bridging J'_b, as well as the bridging capacity σ_0 is listed in Table 6. Matrix parameters, including fracture toughness K_m, Young's Modulus E_m, crack tip toughness J_{tip}, first cracking strength σ_{fc}, and strain-hardening indices (J'_b/J_{tip}, σ_0/σ_{fc}) are also shown.

The $\sigma(\delta)$ curve is modified by RH through the fiber/matrix interfacial properties, particularly the frictional bond τ_0 (Fig. 10). With increasing RH, the rising branch of the $\sigma(\delta)$ curve becomes steeper (Fig. 13), and the complementary energy J'_b diminishes with RH (Table 6).

Usually, high frictional bond during fiber slippage is favorable in maintaining adequate load carrying capacity across multiple cracks [11]. Excessively high frictional bond, however, is not preferred as the strong resistance during fiber debonding and pulling out may cause fiber rupture, thus suppressing the J'_b value [6]. This is supported by the micrographs in Fig. 14. The amount of the ruptured fibers is higher while the length of the protruding fibers is shorter on the failure section of 95% RH cured ECC (Fig. 14(b)) than those of found on the fracture section of the 25% RH cured ECC specimen (Fig. 14(a)).

J_{tip} is found to increase with RH from 14.65 J/m^2 to 20.81 J/m^2 and 14.02 J/m^2 to 17.56 J/m^2 for FA1.2-ECC and FA2.2-ECC, respectively, as shown in Table 6. The increased matrix fracture toughness indicates that more energy is needed to break down the crack tip mortar material when ECC specimen is cured under higher RH. Due to the reduced J'_b and increased J_{tip} at higher RH, J'_b/J_{tip} values decrease with RH (Table 6). The trend of σ_0/σ_{fc} is consistent with that of J'_b/J_{tip}.

The calculated J'_b/J_{tip} and measured tensile ductility are plotted against curing RH in Fig. 15. A consistent trend is observed in a continuous decrease in J'_b/J_{tip} and strain capacity with curing RH. This well explains the higher tensile capacity in ECC cured under low RH. Although high curing RH shows slightly negative influence on tensile strain capacity, the J'_b/J_{tip} and σ_0/σ_{fc} values for all designed ECC exceeded the thresholds for PVA fibers: J'_b/J_{tip} = 3 and σ_0/σ_{fc} = 1.45 as determined by Kanda and Li [38], suggesting that both FA1.2-ECC and FA2.2-ECC cured at RH from 25% to 95% have the potential of multiple cracking behavior.

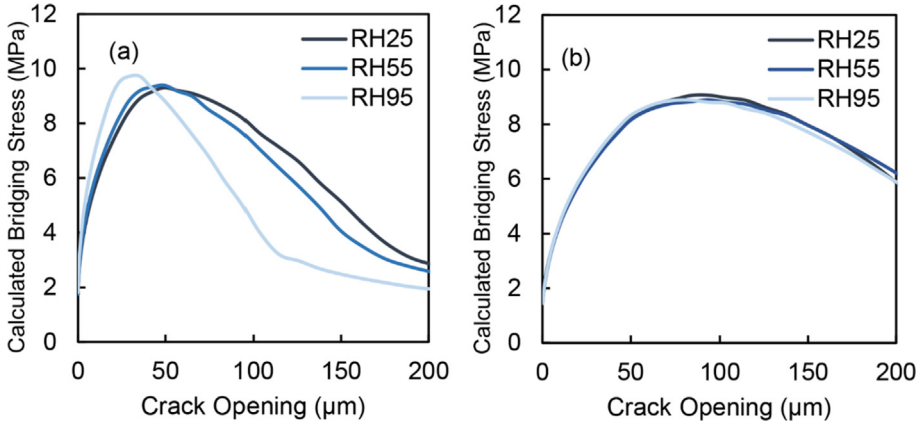

Fig. 13. Computed σ(δ) curves of ECC cured at various curing RH conditions (28d): (a) FA/C = 1.2; (b) FA/C = 2.2. Peak point of $\sigma(\delta)$ curves moves to top-left as RH increases, diminishing J'_b for both ECC mixes.

Table 6
Strain-hardening indices J'_b/J_{tip} and σ_0/σ_{fc} decreases with RH for both ECC mixes.

	FA/C = 1.2							
	E_m GPa	K_m MPa√m	J_{tip} (J/m^2)	J'_b (J/m^2)	J'_b/J_{tip}	σ_0 (MPa)	σ_{fc} (MPa)	σ_0/σ_{fc}
RH25	13.82	0.45	14.65	116.35	7.94	9.30	4.07	2.29
RH55	15.30	0.54	19.06	99.31	5.21	9.39	4.16	2.26
RH95	17.30	0.60	20.81	85.27	4.09	9.72	4.40	2.21
	FA/C = 2.2							
	E_m GPa	K_m MPa√m	J_{tip} (J/m^2)	J'_b (J/m^2)	J'_b/J_{tip}	σ_0 (MPa)	σ_{fc} (MPa)	σ_0/σ_{fc}
RH25	10.30	0.38	14.02	158.48	11.30	9.06	3.96	2.29
RH55	11.30	0.43	16.36	151.14	9.24	8.89	4.05	2.20
RH95	16.00	0.53	17.56	141.73	8.07	8.88	4.71	1.89

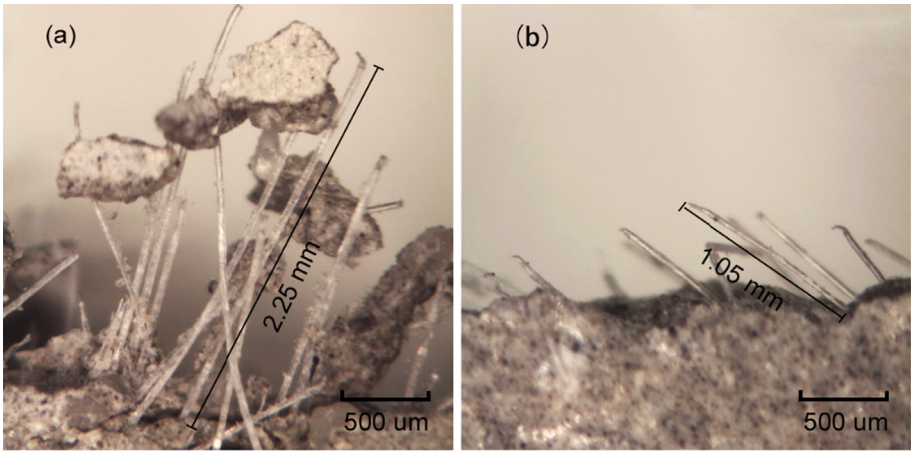

Fig. 14. Micrographs showing protruded fibers on failure section of the FA/C = 1.2 mix (a) RH = 25% and (b) RH = 95%.

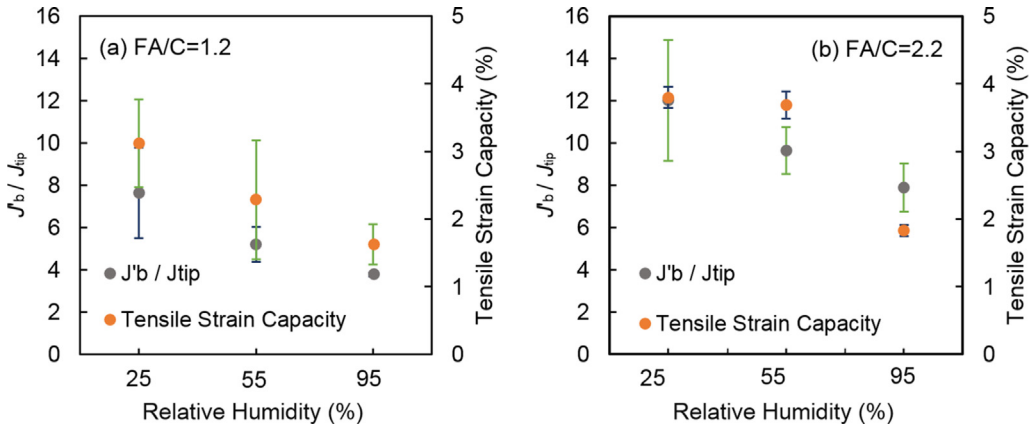

Fig. 15. J'_b/J_{tip} and tensile strain capacity both show strong correlation with curing RH.

The crack number under various RH is also related to changes in J'_b/J_{tip} and σ_0/σ_{fc}. In micromechanics, cracks initiate at flaws and the initiation of cracks is assumed to be determined by the matrix fracture toughness and flaw size [38]. As shown in Fig. 12, the increase of curing RH leads to the increase of the matrix fracture toughness. The high matrix toughness then results in the delay for the initiation of cracks, as supported by the ascending trend of first cracking strength with curing RH (Table 6). On the other hand, the increase of first cracking strength leads to a decrease of σ_0/σ_{fc}, and high toughness (K_m, J_{tip}) generates a low J'_b/J_{tip} This suggests that the margin required to activate more cracks is reduced. Therefore, less crack number is observed both for FA1.2-ECC and FA2.2-ECC cured at higher RH. From the above results, it can be seen that matrix fracture toughness plays a key role in crack initiation, and subsequently, the density of cracks.

The decrease in crack width for specimens cured at low RH may reflect a crack shielding effect when new cracks are formed close to pre-existing cracks in the multiple cracking process [39]. Because of the higher crack density, new cracks initiated from flaws close to preexisting cracks are in their "shadow". Under this situation, the tensile stress needs to rise over a distance from zero at the pre-existing crack face to the ambient applied stress level. New microcracks initiated within this distance will take place at a stress level below that of the ambient load and can be expected to have small crack openings.

4. Conclusions

This study investigates the effect of curing relative humidity (RH) on the tensile properties of ECC laboratory specimens. Based on the experimental and analytical results in this study, it is confirmed that curing RH directly impacts on the tensile characteristics, for both compositions of the ECCs studied. Specifically, the following conclusions can be drawn:

(1) While first cracking and ultimate tensile strength show a general increasing trend with curing RH, the tensile strain capacity of ECC tends to decrease with increasing RH. The effects of curing time on tensile properties are generally consistent with those of RH.
(2) The residual crack width slightly increases with RH. More significantly, crack spacing increases with higher curing RH and longer curing time. The reduction in crack number within the gage length overwhelms the increase in crack width, and is responsible for the diminished tensile strain capacity.
(3) The wider crack spacing induced by curing at higher RH can be fundamentally traced to a combination of measured higher matrix fracture toughness K_m and increased fiber/matrix frictional bond τ_0, resulting in a higher first crack strength σ_{fc} and a lower complimentary energy J'_b. These

changes in the matrix and fiber bridging behavior in response to curing RH lead to the lowering of the strain-hardening indices J'_b/J_{tip} and σ_0/σ_{fc} which in turn limits the saturation of multiple cracking in the ECC. Micromechanical analyses, therefore, offer a fundamental understanding behind the observed macroscopic trends in tensile properties of ECC as influenced by curing RH.

(4) Although high curing RH reduces the tensile strain capacity, all specimens in this study generate robust strain-hardening with multiple cracking. The crack width of all specimens remains less than 50 μm regardless of curing RH, curing time, and FA content.

CRediT authorship contribution statement

Mingfeng Xu: Investigation, Methodology, Writing - original draft, Visualization. **Jing Yu:** Investigation, Methodology. **Jian Zhou:** Validation, Visualization, Writing - review & editing, Supervision. **Yi Bao:** Validation, Writing - review & editing. **Victor C. Li:** Conceptualization, Validation, Writing - review & editing, Supervision.

Declaration of Competing Interest

The authors declare that they have no known competing financial interests or personal relationships that could have appeared to influence the work reported in this paper.

Acknowledgments

Mingfeng Xu greatly appreciates the support provided by China Scholarship Council (CSC), Natural Science Foundation of China (No. 51878238, 51702082), and Jing Yu greatly appreciates the Fulbright program grant sponsored by the Bureau of Educational and Cultural Affairs of the United States, during their visits at the ACE-MRL at the University of Michigan. This research is partially supported by a University of Michigan Distinguished University Professorship.

References

[1] V.C. Li, Engineered cementitious composites (ECC) – material, structural, and durability performance, Concr. Construct. Eng. Handbook (2008) 1–78.
[2] V.C. Li, On engineered cementitious composites (ECC), J. Adv. Concr. Technol. 1 (3) (2003) 215–230.
[3] V.C. Li, Bendable concrete, innovation in construction, Hong Kong Construct. Indust. Council Res. J. (2016) 11–17.
[4] C. Wu, V.C. Li, Thermal-mechanical behaviors of CFRP-ECC hybrid under elevated temperatures, Compos. B Eng. 110 (2017) 255–266.
[5] B. Li, H. Xiong, J. Jiang, X. Dou, Tensile behavior of basalt textile grid reinforced Engineering Cementitious Composite, Compos. B Eng. 156 (2019) 185–200.
[6] S. Wang, V.C. Li, Engineered Cementitious Composites with high-volume fly ash, ACI Mater. J. 104 (3) (2007) 233–241.
[7] E.-H. Yang, Y. Yang, V.C. Li, Use of high volumes of fly ash to improve ECC mechanical properties and material greenness, ACI Mater. J. 104 (6) (2007) 620–628.
[8] J. Yu, C.K. Leung, Strength improvement of strain-hardening cementitious composites with ultrahigh-vlume fly Ash, J. Mater. Civ. Eng. 29 (9) (2017) 05017003.
[9] J. Yu, J. Yao, X. Lin, H. Li, J.Y. Lam, C.K. Leung, I.M. Sham, K. Shih, Tensile performance of sustainable Strain-Hardening cementitious composites with hybrid PVA and recycled PET fibers, Cem. Concr. Res. 107 (2018) 110–123.
[10] V.C. Li, Engineered Cementitious Composites (ECC): Bendable Concrete for Sustainable and Resilient Infrastructure, Springer, 2019.
[11] V.C. Li, Tailoring ECC for special attributes: A review, Int. J. Concr. Struct. Mater. 6 (3) (2012) 135–144.
[12] A.A. Ramezanianpour, V.M. Malhotra, Effect of curing on the compressive strength, resistance to chloride-ion penetration and porosity of concretes incorporating slag, fly ash or silica fume, Cem. Concr. Compos. 17 (2) (1995) 125–133.
[13] P. Amorim, J. De Brito, L. Evangelista, Concrete made with coarse concrete aggregate: influence of curing on durability, ACI Mater. J. 109 (2) (2012) 195–204.
[14] J.A. Hanson, Effects of curing and drying enviroments on splitting tensile strength of concrete, Am. Concr. Inst. J. 65 (7) (1968) 535–543.
[15] R.G. Patel, L.J. Parrott, J.A. Martin, D.C. Killoh, Gradients of microstructure and diffusion properties in cement paste caused by drying, Cem. Concr. Res. 15 (2) (1985) 343–356.
[16] P. Mehta, M. PJM, Concrete: microstructure, properties, and materials, New York, 2005.
[17] R. Ranade, J. Zhang, J.P. Lynch, V.C. Li, Influence of micro-cracking on the composite resistivity of engineered cementitious composites, Cem. Concr. Res. 58 (2014) 1–12.
[18] M. Ohno, V.C. Li, A feasibility study of strain hardening fiber reinforced fly ash-based geopolymer composites, Constr. Build. Mater. 57 (2014) 163–168.
[19] H. Liu, Q. Zhang, V. Li, H. Su, C. Gu, Durability study on engineered cementitious composites (ECC) under sulfate and chloride environment, Constr. Build. Mater. 133 (2017) 171–181.
[20] M. Lepech, V.C. Li, Long term durability performance of engineered cementitious composites/Langzeitbeständigkeit systematisch entwickelter zusammengesetzter Zement gebundener Werkstoffe, Restor. Build. Monu. 12 (2) (2006) 119–132.
[21] M. Şahmaran, V.C. Li, Durability of mechanically loaded engineered cementitious composites under highly alkaline environments, Cem. Concr. Compos. 30 (2) (2008) 72–81.
[22] H. Liu, Q. Zhang, C. Gu, H. Su, V.C. Li, Influence of micro-cracking on the permeability of engineered cementitious composites, Cem. Concr. Compos. 72 (2016) 104–113.
[23] ASTM, Standard test method for flow of hydraulic cement mortar, West Conshohocken, PA, 2015.
[24] ASTM, Standard test method for compressive strength of hydraulic cement mortars, Annual Book of ASTM Standards, 2013, pp. 1-9.
[25] J.C. Committee, Recommendations for design and construction of high performance fiber reinforced cement composites with multiple fine cracks, Japan Society of Civil Engineers, Tokyo, Japan, 2008.
[26] X. Huang, R. Ranade, W. Ni, V.C. Li, On the use of recycled tire rubber to develop low E-modulus ECC for durable concrete repairs, Constr. Build. Mater. 46 (2013) 134–141.
[27] M. Li, V.C. Li, Cracking and healing of engineered cementitious composites under chloride environment, ACI Mater. J. 108 (3) (2011) 333–340.
[28] V.C. Li, C. Wu, S. Wang, A. Ogawa, T. Saito, Interface tailoring for Strain-Hardening polyvinyl alcohol-Engineered CementitiousComposite (PVA-ECC), ACI Mater. J. 99 (5) (2002) 463–472.
[29] J. Zhou, S. Qian, M.G.S. Beltran, G. Ye, K. van Breugel, V.C. Li, Development of Engineered Cementitious Composites with limestone powder and blast furnace slag, Mater. Struct. 43 (6) (2010) 803–814.
[30] C. Redon, V.C. Li, C. Wu, H. Hoshiro, T. Saito, A. Ogawa, Measuring and modifying interface properties of PVA fibers in ECC matrix, J. Mater. Civ. Eng. 13 (6) (2001) 399–406.
[31] ASTM, Standard test method for linear-elastic plane-strain fracture toughness Klc of metallic materials, West Conshohocken, PA., 2012.
[32] B. Lothenbach, K. Scrivener, R. Hooton, Supplementary cementitious materials, Cem. Concr. Res. 41 (12) (2011) 1244–1256.
[33] Y. Yang, M.D. Lepech, E.-H. Yang, V.C. Li, Autogenous healing of engineered cementitious composites under wet–dry cycles, Cem. Concr. Res. 39 (5) (2009) 382–390.
[34] G.P. van Zijl, V. Slowik, R.D. Toledo Filho, F.H. Wittmann, H. Mihashi, Comparative testing of crack formation in strain-hardening cement-based composites (SHCC), Mater. Struct. 49 (4) (2016) 1175–1189.
[35] V.C. Li, H.-C. Wu, Conditions for pseudo strain-hardening in fiber reinforced brittle matrix composites, J. Appl. Mech. Rev. 45 (8) (1992) 390–398.
[36] E.-H. Yang, Designing Added Functions in Engineered Cementitious Composites, University of Michigan, Ann Arbor, 2008.
[37] H. Ma, J. Cai, Z. Lin, S. Qian, V.C. Li, $CaCO_3$ whisker modified Engineered Cementitious Composite with local ingredients, Constr. Build. Mater. 151 (2017) 1–8.
[38] S. Wang, Micromechanics based matrix design for Engineered Cementitious Composites, University of Michigan, MI, USA, 2005.
[39] C. Lu, C.K. Leung, V.C. Li, Numerical model on the stress field and multiple cracking behavior of Engineered Cementitious Composites (ECC), Constr. Build. Mater. 133 (2017) 118–127.